Am J Cancer Res 2023;13(10):4547-4559
www.ajcr.us /ISSN:2156-6976/ajcr0152143

Original Article

Superiority of FAPI-PET/CT for examining multiple malignant tumors: a retrospective study

Wei Li, Zhiyun Jiang, Nan Cui, Jiatong Li, Liang Cheng, Wei Liu, Jing Li, Kezheng Wang

Department of PET-CT/MRI, Harbin Medical University, Harbin Medical University Cancer Hospital, Harbin 150081, Heilongjiang, China

Received July 10, 2023; Accepted August 29, 2023; Epub October 15, 2023; Published October 30, 2023

Abstract: To compare the diagnostic value of [^{18}F]-AlF-NOTA-FAPI-04 PET/CT and [^{18}F]-FDG PET/CT for primary and metastatic lesions in different types of tumors. A retrospective analysis was conducted on 51 patients with 11 different types of tumors. Among them, 20 patients underwent PET/CT, and 31 patients underwent restaging. The patients were diagnosed using [^{18}F]-AlF-NOTA-FAPI-04 PET/CT and [^{18}F]-FDG PET/CT scan techniques, and adverse reactions were recorded. Thickness of primary lesions, metastasis, and lymph node involvement were analyzed and confirmed by histological analysis. The sensitivity, specificity, positive predictive value, negative predictive value, and accuracy of [^{18}F]-AlF-NOTA-FAPI-04 PET/CT and [^{18}F]-FDG PET/CT were calculated. Neither [^{18}F]-AlF-NOTA-FAPI-04 PET/CT nor [^{18}F]-FDG PET/CT scan techniques caused adverse reactions in the patients. [^{18}F]-AlF-NOTA-FAPI-04 PET/CT performed well in detecting recurrence, with a positive rate of 100%, higher than 71.0% of [^{18}F]-FDG PET/CT. Compared with [^{18}F]-FDG PET/CT, [^{18}F]-AlF-NOTA-FAPI-04 PET/CT identified 6 types of malignant tumors more clearly, and could improve the detection rate of primary and metastatic tumors (97.0% vs. 84.8%, $P<0.001$). [^{18}F]-AlF-NOTA-FAPI-04 PET/CT exhibited a higher sensitivity for detecting lymph node (81.8% vs. 50.0%, $P<0.05$) than [^{18}F]-FDG PET/CT. Additionally, [^{18}F]-AlF-NOTA-FAPI-04 PET/CT demonstrated higher diagnostic sensitivity (67.39% vs. 58.7%, $P=0.387$) and accuracy (82.14% vs. 60.71%, $P=0.377$) for detecting metastatic lesions compared to [^{18}F]-FDG PET/CT. [^{18}F]-AlF-NOTA-FAPI-04 PET/CT outperforms [^{18}F]-FDG PET/CT in diagnosing primary and metastatic lesions across various types of tumors, especially in identifying lymph node, visceral, and peritoneal metastases. It can improve diagnostic efficiency and accuracy, thereby positively influencing clinical decision-making for optimal patient management.

Keywords: [^{18}F]-AlF-NOTA-FAPI-04 PET/CT, [^{18}F]-FDG PET/CT, lymph node metastasis, bone and visceral metastasis, peritoneal metastasis

Introduction

Malignant tumors consist of tumor cells as well as a variety of non-malignant cells that contribute to the formation and composition of tumor mesenchymal microenvironment [1]. In certain cancers, imaging techniques that focus on the tumor cells are less sensitive than mesenchymal-targeted imaging, as the mesenchyme accounts for 90% of the total volume of the tumor [2]. Cancer-associated fibroblasts (CAFs) are a heterogeneous population of cells that constitute the majority of the tumor mesenchyme. They play a critical role in tumor enlargement, metastasis, migration, extracellular matrix remodeling, therapy resistance, and immunosuppression [3]. Compared to cancer cells, genetically, CAFs are more stable and less prone to therapeutic resistance, making them ideal target cells for antitumor therapy [4]. The development of CAFs in the tumor mesenchyme is accompanied by alterations in morphology and the production of specific surface markers, including fibroblast activation protein (FAP). According to the research, FAP is intensely expressed in over 90% of mesenchyme in epithelial carcinoma [5, 6].

FAP, a membrane-bound glycoprotein of type II, belongs to the family of dipeptidyl peptidases 4 (DPP4). It possesses both dipeptidyl peptidase and endopeptidase activities and shares a protein-level homology of 52% with DPP4. FAP expression is observed only in inactivated fibro-

blasts, not in quiescent fibroblasts [7]. CAFs are strongly expressed in several epithelial malignancies, particularly hepatocellular, colorectal, ovarian, and pancreatic cancers, characterized by a strong pro-fibroproliferative response [8]. The correlation between the poor prognosis in tumor patients and FAP overexpression revealed that FAP activity affects the tumor development, metastasis, and invasion [9]. The relatively distinctive expression of FAP differentiates CAFs from ordinary fibroblasts [10]. Therefore, FAP-targeted imaging is currently considered to be a promising strategy for tumor-stromal visualization. [18F]-AIF-NOTA-FAPI-04 imaging works based on the overexpression of αVβ3 and αVβ5 integrins on the surface of tumor cells, while [18F]-FDG PET detects the differences in metabolic activity between tumor cells and surrounding normal tissues. In recent years, PET/CT imaging targeting tumor mesenchymal FAP has gained significant research attention worldwide. The currently reported imaging agent [68Ga]-FAPI-04 has shown promising results in the pre-treatment staging and post-treatment evaluation of a wide range of tumors. However, probes, such as [68Ga]-FAPI-04, are limited by short half-lives and low preparation volumes. Typically, there is only enough drug for 1 to 3 patients per production run. The cost of the [68Ge]/[68Ga] generator and the lower resolution of [68Ga] PET imaging should also be taken into account. As the other most commonly used posionuclide in clinical practice, [18F] (radioactive half-life =109.8 min) can be produced in large quantities by a cyclotron. [18F]-labeled FAPI probes have offer more favorable characteristics, including suitable half-lives, high radioactivity yields, and high purity of radiochemistry. These probes demonstrate good pharmacokinetics and tumor absorption in both tumor individuals and normal models. Additionally, [18F]-labeled FAPI probes allow for delayed visualization as well as the potential for multiple patient detections. The recent progress in radiolabeling of FAPI probes with [18F] has shown promise in clinical and preclinical research [11, 12]. There is significant heterogeneity among different types of cancers, with differences in tumor surface markers, metabolic levels, or growth characteristics. Currently, it is difficult to detect different cancers at the same time with a single test. Therefore, different diagnostic methods are needed for discrimination and judgement, which significantly increases medical costs. In this study, we aim to apply [18F]-AIF-NOTA-FAPI-04 PET/CT and [18F]-FDG PET/CT in the diagnosis of primary and metastatic lesions of various tumors, such as lung cancer, liver cancer, gastric cancer, ovarian cancer, pancreatic cancer, prostate cancer, colorectal cancer, esophageal cancer, cervical cancer, breast cancer, and renal cancer. We aimed to investigate the clinical application value of [18F]-AIF-NOTA-FAPI-04 PET/CT and [18F]-FDG PET/CT in the diagnosis and differentiation of various tumors, so as to provide a clinical basis for tumor diagnosis and expand the options for tumor evaluation.

Materials and methods

Study design and patients

The data collected in this study have no harm to the subjects' interests, and the study protocol has been approved by the Institutional Review Committee of the Cancer Hospital of Harbin Medical University.

All 51 patients were recommended by clinical oncologists and admitted to Harbin Medical University Cancer Hospital between May 2021 to January 2022. The [18F]-AIF-NOTA-FAPI-04 PET/CT was applied after the [18F]-FDG PET/CT for comparison, without changing the final management of the patients. Inclusion criteria: (1) patients who were diagnosed with any kind of malignant tumor (including but not limited to lung cancer, liver cancer, gastric cancer, ovarian cancer, pancreatic cancer, prostate cancer, colorectal cancer, esophageal cancer, cervical cancer, breast cancer, and renal cancer); (2) patients who underwent [18F]-AIF-NOTA-FAPI-04 PET/CT and [18F]-FDG PET/CT examinations; (3) patients whose diagnosis was subsequently confirmed by pathological examination; (4) patients who agreed to use their medical records and examination results for research; (5) patients whose missing important medical records or examination results was rectified. Exclusion criteria: (1) patients with poor quality of PET/CT examination results, e.g., significant masses or artifacts that affected the lesion detection or evaluation; (2) patients missing essential medical records or examination results, such as laboratory or histopathological results, operation reports and drug treatment records; (3) patients who received radiothera-

py, chemotherapy or living surgery before PET/CT examinations.

[18F]-AIF-NOTA-FAPI-04 and [18F]-FDG preparation

FDG was prepared according to a standard method using F300e chemical synthesis module (Sumitomo, Japan). The FAPI precursor (AIF-NOTA-FAPI-04) was acquired from Nanchang Probe Biotechnology Co.

To prepare buffer solution, 0.9 g of NaAc was dissolved into 100 m of water. While measuring the pH of the solution, HAc was added dropwise until the pH reduced to 4.0 (approximately 1.2 mL of HAc was used). To prepare aluminum trichloride solution, 0.2415 g of $AlCl3.6H_2O$ was dissolved in 100 mL of injection water to prepare 10 mmol/L of aluminum trichloride solution. Next, 1 mg of AIF-NOTA-FAPI precursor chemistry was place in a cillin vial, and 500 μL of acetonitrile and 500 μL of L1.1 buffer were added to the cillin vial with a pipette to sonicate the precursor. Then, 200 μL of the 2.1 precursor solution was add to a 3 ml Celine bottle, along with 10 μL of aluminum trichloride solution. Another 300 μL of acetonitrile and 225 μL of buffer solution was added to the bottle. The ^{18}F- was obtained by bombarding of heavy oxygen water with the accelerator, and then it was passed into the CFN200 synthesis module. The QMA column was used to capture and record the RI1 activity. Bottles of saline were added to the reaction tube, the reaction solution was dissolved and placed on an ^{18}C column for capturing the product. The reaction tube was washed with saline, and the ^{18}C column was cleaned. To extract the desired product, membrane filtration was performed. Pump A, which contained a solution consisting of 0.25% methanol and 0.08% trifluoroacetic acid, and pump B, which contained 0.75% water, were used to maintain a constant flow rate of 1 ml/min, ensuring that the column temperature matched the room temperature. For quality control purposes, the retention time was set at 5.15 min.

Procedures related to PET/CT imaging

A paired PET/CT scans with [18F]-AIF-NOTA-FAPI-04 and [18F]-FDG were applied within 7 days. Patients were required to fast for at least five hours before the PET/CT scan with [18F]-FDG. Before undergoing a CT scan, they were instructed to drink 500 mL of water to facilitate the excretion of [18F]-FDG from the kidney calyces and promote urination. Prior to the [18F]-FDG PET/CT assessment, it was ensured that the patient's peripheral blood glucose levels were normal. Based on patient weight, the intravenous [18F]-FDG versus [18F]-AIF-NOTA-FAPI-04 doses were calculated (3.7 MBq for FDG and 1.8-2.2 MBq for FAPI). Data were acquired using a hybrid PET/CT system (Discovery 690, GE Healthcare, Milwaukee, USA) after 1-hour intravenous administration. For [18F]-FDG, an upper-thigh CT scan (head scan alone) was applied, and for [18F]-AIF-NOTA-FAPI-04, the scan was from head to upper thigh. The CT scanning parameters were set as follows, tube voltage: 110 kV, tube current: 120 mA, and slice thickness: 3.75 mm. Following the CT scan, a PET scan was immediately carried out with 6-8 beds and a duration of 2.0 to 2.5 minutes per position in a 3D acquisition mode. Acquired data were transferred to Advantage Workstation (version AW4.7, GE Healthcare, Milwaukee, WI, USA). Data were reconstructed using the ordered subset expectation maximization algorithm (2 iterations/21 subsets), with CT attenuation correction. After reconstruction, co-aligned images were displayed. Patients were instructed by the clinical physician to report any changes in vital signs, including heart rate, breathing, blood pressure, or temperature, within 120 minutes after the PET/CT scan following the injection of [18F]-AIF-NOTA-FAPI-04.

Review of PET/CT imaging

Two experienced radiologists analyzed the images from the [18F]-FDG and [18F]-AIF-NOTA-FAPI-04 PET/CT scans. To prevent bias, PET/CT images of [18F]-FDG were reviewed by Zhiyun Jiang, and PET/CT images of [18F]-AIF-NOTA-FAPI-04 were reviewed by Kezheng Wang. The image evaluations were conducted without the information available from other PET/CT scans. Viewing of the PET/CT fusion was performed using the Advantage workstation (AW4.7, GE Healthcare). Around the tumor lesion on the transexual image, a region of interest was drawn for semi-quantitative analysis. The maximum standard uptake values (SUVmax) were automatically calculated for quantifying the uptake of the tracer in primary tumors, lymph nodes, and metastases. For measuring the

lymph nodes, primary tumors, and metastases tracer uptake, SUVmax was utilized. For brain lesions, the SUVmax value of the lesion was divided by the average SUV value (SUVmean) of the contralateral normal tissue. The tumor-to-background (T/B) ratio was calculated to determine individual lymph nodes and primary lesions in the liver, brain, peritoneum, lung, bone, and pleura. Lesions were considered positive if they had more cell activity than surrounding tissues. There were five sites where lymph nodes were categorized individually, comprising supraclavicular, axillary, neck, mediastinal (comprising diaphragmatic, intramammary, epicardial, and hilar lymph nodes), abdominal (including para-aortic, retroperitoneal, mesenteric, abdominal and iliac regions). There were separate categories for the involvement of the bone, pleura, peritoneum, liver, lung, and brain. Using [18F]-FDG and [18F]-AIF-NOTA-FAPI-04, we recorded the SUVmax, median, and range for each site. In the case of multiple positive lesions at a single site, the SUV values of the five most active lesions (>5) or the SUV values of all lesions (≤5) were averaged to obtain a final SUV value.

Statistical analysis

The data in this study were statistically analyzed by R software version 4.0.3. To compare the means of two continuous variables that were normally distributed (mean ± SD), independent samples t-tests were employed. For comparing two groups of non-normally distributed variables (median, IQR), the Mann-Whitney Index U test was utilized. Pearson χ^2 and McNemars tests were employed to compare the frequencies of the categorical variables. Classification performance was evaluated by confusion matrix analysis and receiver operating characteristic (ROC) curves. For visceral and lymph node metastases recognized by [18F]-FDG and [18F]-AIF-NOTA-FAPI-04, the diagnostic values were analyzed and compared. $P<0.05$ was considered significant.

Results

Overview of clinical characteristics of the patients

Among the 51 patients, there were 23 males and 28 females. The ages of the subjects ranged from 33 to 81 years old, with an average of 59 years. The patients were diagnosed with 11 types of cancer, including lung, liver, stomach, ovarian, pancreatic, prostate, colorectal, esophageal, cervical, breast and kidney cancers. Of these, 20 newly diagnosed patients received a preliminary PET/CT assessment for lesion detection and staging, and 31 patients with recurrent tumors underwent PET/CT scans for restaging. A total of 11 types of cancers were identified. The research design is shown in **Figure 1**.

Out of 20 newly diagnosed patients, the clinical staging suggested by [18F]-AIF-NOTA-FAPI-04 PET/CT was higher than that of [18F]-FDG PET/CT. Positive rates for [18F]-FDG PET/CT and [18F]-AIF-NOTA-FAPI-04 PET/CT were 71.0%, and 100%, respectively, among patients undergoing recurrence detection. See **Table 1** for details.

Adverse events

All patients were able to endure the [18F]-AIF-NOTA-FAPI-04 PET/CT scan. The adverse effects of the medication were not observed. No vital indicators (including temperature, heart rate, and blood pressure) were observed to be altered within hours after the injection. There were no other symptoms reported by the patients.

Primary cancer detection

There were 2 patients with 2 primary lesions, 4 patients with 3 primary lesions, and 1 patient with 4 primary lesions among the 20 newly diagnosed patients (a total of six types of c). Thus, we examined 33 primary lesions. We compared the semi-quantitative parameters of [18F]-AIF-NOTA-FAPI-04 and [18F]-FDG in primary tumors. See **Figure 2**.

In primary tumors, the [18F]-FDG PET/CT sensitivity was 84.8% (28 out of 33), while that of [18F]-AIF-NOTA-FAPI-04 PET/CT was 97.0% (32 out of 33) ($P<0.001$). Five cases of liver cancer (3 cases), gastric cancer (1 case), and lung cancer (1 case) were not seen by the [18F]-FDG PET/CT. In [18F]-AIF-NOTA-FAPI-04 PET/CT images, most primary lesions had obvious tumor contours and a greater tumor background ratio, when compared to [18F]-FDG, particularly in hepatocellular carcinoma, pancreatic cancer (**Figure 3**), and neuroglioma.

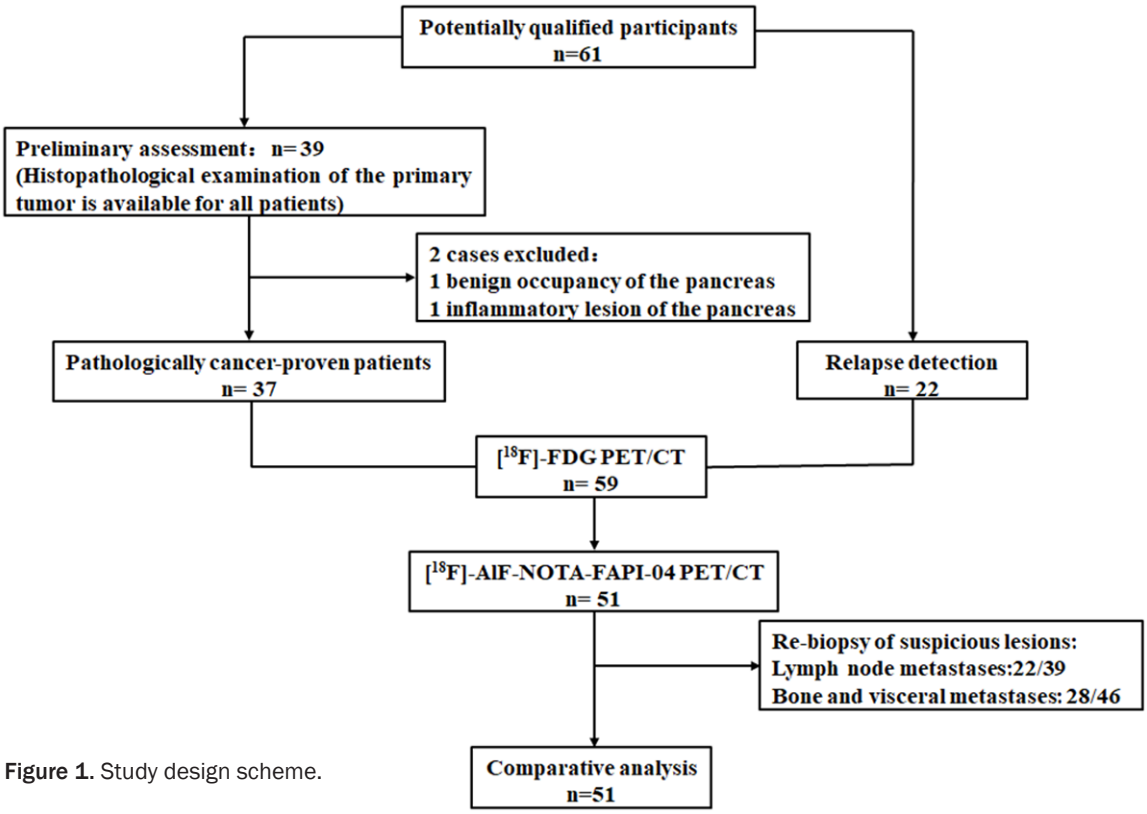

Figure 1. Study design scheme.

Table 1. Comparison of initial staging and recurrence detection results

Initial staging	N	[18F]-FDG PET/CT staging				[18F]-FAPI-04 PET/CT staging			
Type of cancer		I	II	III	IV	I	II	III	IV
Total	20	7		2	11	5	1	1	13
Lung ca	3			1	2			1	2
Liver ca	7	2			5	1			6
Stomach ca	4	2		1	1	1	1		2
Ovarian ca	2				2				2
Pancreatic ca	3	3				3			
Prostate ca	1				1				1
Recurrence detection	N	[18F]-FDG PET/CT staging				[18F]-FAPI-04 PET/CT staging			
Cancer type		Negative		Positive		Negative		Positive	
Total	31	9		22				31	
Lung ca	2			2				2	
Colorectal ca	7	2		5				7	
Liver ca	4	2		2				4	
Stomach ca	4	1		3				4	
Ovarian ca	3			3				3	
Pancreatic ca	2	1		1				2	
Breast ca	3	1		2				3	
Cervical ca	2			2				2	
Kidney ca	2	1		1				2	
Prostate ca	1	1						1	
Esophageal ca	1			1				1	

Note: Clinical staging is based on the American Joint Committee on Cancer (AJCC) staging system (8th edition). Ca: cancer.

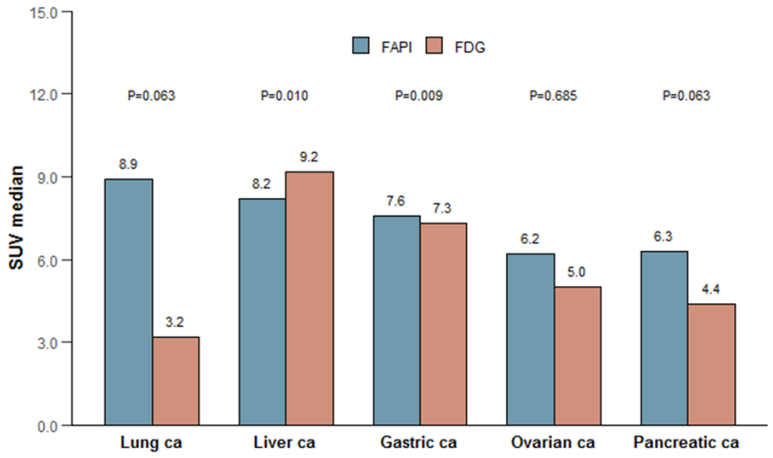

Figure 2. Differences in semi-quantitative parameters of [18F]-AIF-NOTA-FAPI-04 and [18F]-FDG in primary tumors. Note: The size of gastric and colorectal cancers is indicated by the thickness of the primary lesion. The size of other types of cancer is expressed as the largest diameter of the primary lesion.

Lymph node metastases detection

PET-positive lymph nodes were categorized into 5 categories based on their anatomical sites among the 20 newly diagnosed patients. Since some patients had lymph nodes that were positive in the axillary and inguinal sites, 4 regions were finally assessed in this study (the hilar region was classified within the mediastinum, and the iliac region was classified within the abdomen). As shown in **Table 2**, lymph nodes in 4 sites (cervical, supraclavicular, abdomen, oral, and mediastinal) revealed higher SUV median and range in [18F]-AIF-NOTA-FAPI-04 than in [18F]-FDG (all $P<0.05$) (**Figure 4**).

In total, 39 lymph nodes were found in 16 patients, and pathological information was used to assess the lymph nodes. Of these, 22 lymph nodes in 12 patients were confirmed to be malignant. Based on the data obtained from [18F]-AIF-NOTA-FAPI-04 PET/CT, lymph node interference in 12 of the 16 patients was correctly identified (false-negative in 1 patient and false-positive in 3 patients). Based on [18F]-FDG PET/CT information, the involvement of lymph nodes was determined in 8 of the 16 patients (6 false negatives and 2 false positives).

The sensitivity, specificity, positive predictive value (PPV), negative predictive value (NPV), and accuracy of [18F]-FDG PET/CT in the diagnosis of metastatic lymph nodes were 50.0%, 70.59%, 68.75%, 52.17%, and 58.97%, respectively, and those of [18F]-AIF-NOTA-FAPI-04 PET/CT were 81.82%, 58.82%, 72%, 71.43%, and 71.79%, respectively (**Table 3**). The accuracy and sensitivity of [18F]-AIF-NOTA-FAPI-04 PET/CT were higher (sensitivity, $P=0.026$; accuracy, $P=0.234$). The specificity of [18F]-FDG PET/CT was higher, but the difference was not statistically significant ($P=0.472$). However, there was no significant difference in specificity and good consistency (**Table 4**).

Bone and visceral metastases detection

Aberrant lesions in the pleura, lung, omentum, peritoneum, bone, and liver were divided into separate areas to assess the value of [18F]-AIF-NOTA-FAPI-04 and [18F]-FDG PET/CT to detect bone and visceral metastases (**Figure 5**). Compared to [18F]-FDG, [18F]-AIF-NOTA-FAPI-04 demonstrated a higher detection rate of metastatic foci and exhibited higher tracer uptake levels, as demonstrated in **Table 5**. In addition, [18F]-AIF-NOTA-FAPI-04 revealed identified more abnormal lesions compared to [18F]-FDG, particularly in the liver, retroperitoneum, omentum, mesentery (**Figure 6**), brain and skull (**Figure 7**), and axial bone.

Distant metastases were identified by the biopsy (CT or ultrasound-guided percutaneous aspiration biopsy or laparoscopic biopsy) in 46 lesions among 32 patients. As a result, 28 metastatic lesions were confirmed in 22 patients. In 26 of the 32 patients, metastatic lesions were accurately identified using [18F]-AIF-NOTA-FAPI-04 PET/CT (2 false negatives and 4 false positives), but [18F]-FDG PET/CT data presented correct diagnosis in 16 of the 32 patients (4 false positives and 12 false negatives). The main false-positive uptake of [18F]-AIF-NOTA-FAPI-04 PET/CT was related to inflammatory disease (2 cases), fibrotic nodules (1 case), and myelofibrosis (1 case). **Table 6** summarizes the specificity, sensitivity, NPV, PPV, and accuracy of lesion analysis-based identification of metastatic lesions. In terms of sensitivity, [18F]-FDG PET/CT has an advantage over [18F]-FAPI-04 PET/CT, with a general consistency between the two tests. There was no significant differ-

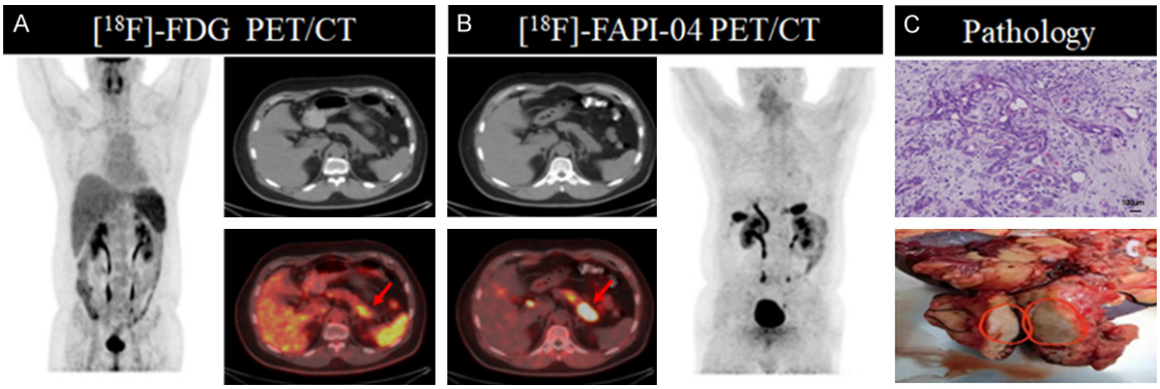

Figure 3. Results of pancreatic cancer examination. A 43-year-old man had abdominal pain for 2 months and elevated CA199 level. He self-reported that pancreatic MRI revealed a suspected malignant tumor occupying the pancreatic tail. Further evaluation with [18F]-FDG PET/CT and [18F]-FAPI-04 PET/CT was performed before treatment. A. [18F]-FDG PET/CT images demonstrated pancreatic tail occupancy with SUVmax: 6.5. B. [18F]-FAPI-04 PET/CT images displayed pancreas tail occupancy with SUVmax: 22.7. In addition, the pancreatic body inflammation was very clear. C. Surgical pathology indicated a moderately differentiated ductal adenocarcinoma of the pancreas, Scale bar, 100 μm.

Table 2. Comparison of [18F]-AIF-NOTA-FAPI-04 and [18F]-FDG performance and semi-quantitative parameters of lymph nodes

Department	Lymph node size (cm)		Tracer	No. of positive	SUV median	SUV range	*P*-value
	Median	Range		Cases (patients)			
Neck	2.00	0.9-3.5	FDG	5	3.45	1.2-8.8	0.009
			FAPI	8	6.6	1.7-9.8	
Supraclavicular	2.50	0.6-4.0	FDG	6	5.35	1.5-9.3	0.014
			FAPI	9	6.65	4.1-10.8	
Mediastinum (Incudes epicardium, internal breast, diaphragm and hilar)	2.15	0.8-3.0	FDG	7	3.55	0.7-8.9	<0.001
			FAPI	11	6.45	2.1-11.9	
Abdomen (Incudes Aorta parietal, hilar, retroperitoneal, abdominal and iliac regions)	2.05	0.8-3.2	FDG	14	1.85	0.5-8.2	0.001
			FAPI	23	3.1	1.3-10.4	

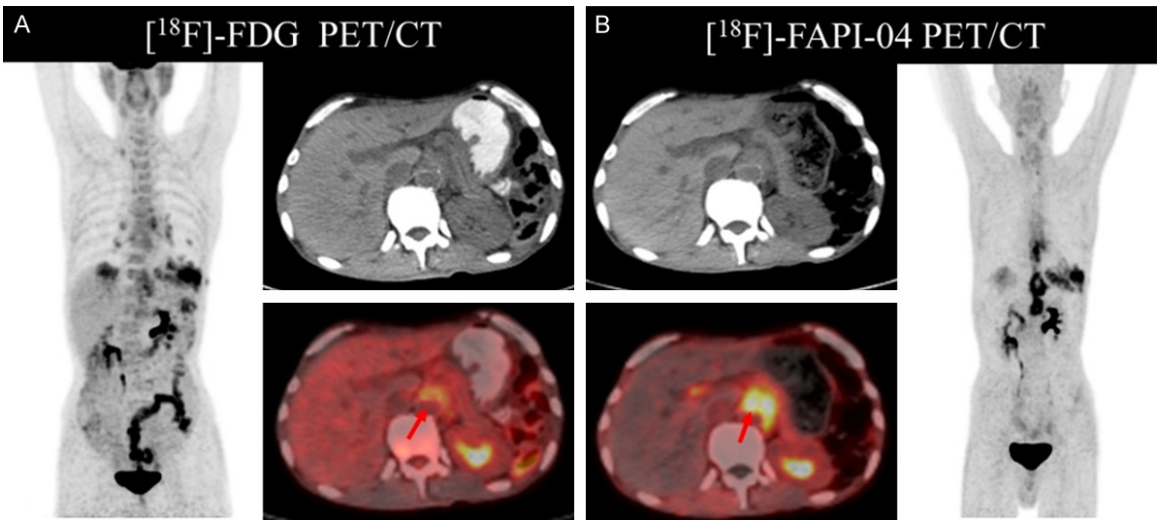

Figure 4. Detection results of lymph node metastasis. A 59-year-old man who had a one-month history of food choking, with a history of for cardia esophagus cancer surgery two years ago, without radiotherapy. Gastroscopy revealed inflammatory changes around the anastomosis. [18F]-FDG PET/CT images revealed hyperintensity mass around the anastomotic stoma of the esophageal operation area to the posterior pancreatic para-aortic area, fused into a mass (SUVmax: 3.8). [18F]-FAPI-04 PET/CT showed a clearer border of the mass extension (SUVmax: 8.72) compared to [18F]-FDG PET/CT, considering lymph node metastases. FAPI imaging uptake was significantly higher than FDG imaging in terms of the number of lymph node metastases and SUV uptake values.

Table 3. Diagnostic value of [18F]-FAPI-04 PET/CT and [18F]-FDG PET/CT for lymph node involvement

Basis of analysis and modality	Sensitivity (%) 95% CI	Specificity (%) 95% CI	PPV (%) 95% CI	NPV (%) 95% CI	Accuracy (%) 95% CI
[18F]-FDG PET/CT	50.0 (11/22)	70.59 (12/17)	68.75 (11/16)	52.17 (12/23)	58.97 (23/39)
	28.8-71.2	44.0-88.6	41.5-87.9	31.1-72.6	42.1-74.4
[18F]-FAPI-04 PET/CT	81.82 (18/22)	58.82 (10/17)	72.0 (18/25)	71.43 (10/14)	71.79 (28/39)
	58.9-94.0	33.5-80.6	50.4-87.1	42.0-90.4	55.1-85.0
P-value	0.026	0.472	0.823	0.300	0.234

Table 4. Results of the 3-dimensional paired chi-square test for the comparison of lymph node involvement

Item	Sensitivity		Specificity	
	McNemar Test	Kappa	McNemar Test	Kappa
[18F]-FDG PET/CT vs. [18F]-FAPI-04 PET/CT	P=0.016	0.364	P=0.500	0.746

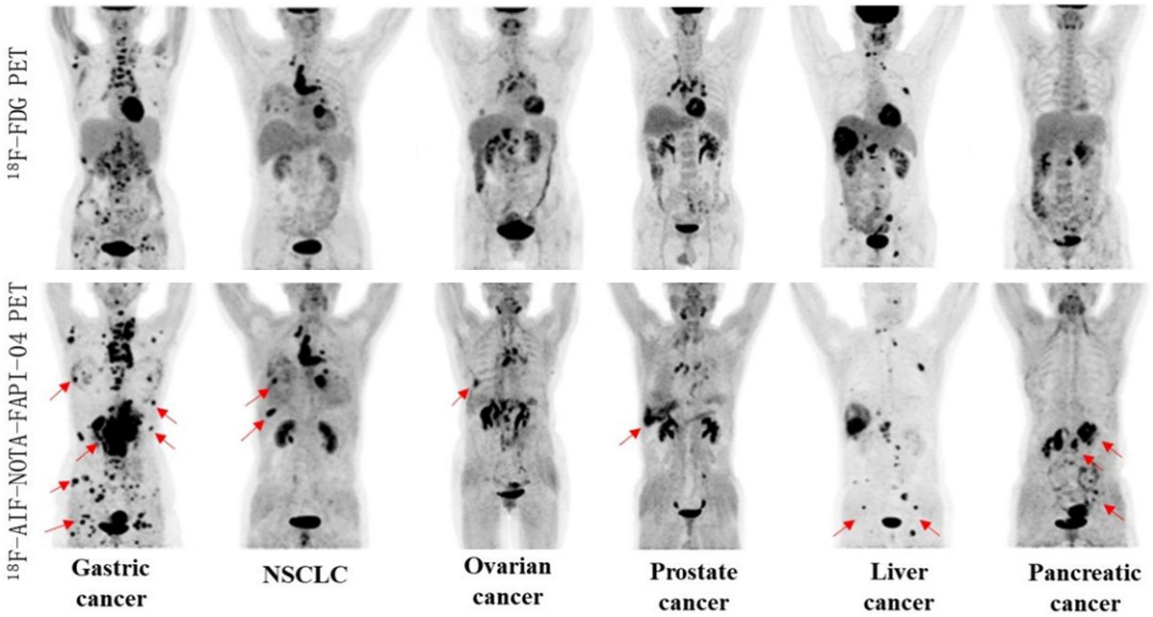

Figure 5. Detection results of metastatic tumor by different methods. Images of 6 patients undergoing [18F]-FDG and [18F]-AIF-NOTA-FAPI-04 PET/CT. The number of metastases in FAPI imaging was significantly higher than that in FDG images.

ence in the specificity between the two tests, and showing good consistency (**Table 7**).

Discussion

This study assessed diagnostic efficacy of the [18F]-FDG PET/CT and [18F]-AIF-NOTA-FAPI-04 PET/CT among multiple small cancer patient groups. [18F]-AIF-NOTA-FAPI-04 PET/CT distinguished 6 types of malignant tumors with a greater rate of primary tumor identification in comparison with the [18F]-FDG PET/CT. Regarding identification of metastatic lesions in patients with newly diagnosed cancer, [18F]-FDG PET/CT revealed a poorer sensitivity in comparison with [18F]-AIF-NOTA-FAPI-04 PET/CT. In addition, the uptake values of [18F]-AIF-NOTA-FAPI-04 in primary and metastatic lesions were significantly higher.

[18F]-AIF-NOTA-FAPI-04 PET/CT successfully detected almost all primary lesion categories (32 out of 33 primary lesions), while [18F]-FDG PET/CT missed 5. This improved detection may

Table 5. Comparison of the performance and semi-quantitative parameters of [18F]-FAPI-04 and [18F]-FDG in bone and visceral metastases

Department	Trace	Number of positive cases (patients)	SUV median	SUV range	*P*-value
Pleura	FDG	3	3.1	1.1-12.9	0.250
	FAPI	5	5.6	1.3-10.5	
Peritoneum	FDG	11	3.93	1.3-17.6	0.001
	FAPI	15	8.6	2.11-17.3	
Lung	FDG	6	3.82	1.4-15.1	0.021
	FAPI	8	5.9	1.6-10.9	
Liver	FDG	6	2.0	1.2-11.9	<0.001
	FAPI	8	7.3	1.1-15.6	
Pancreas	FDG	4	1.5	1.2-2.1	0.125
	FAPI	5	3.85	3.3-9.8	
Hip	FDG	3	2.4	1.0-3.8	0.003
	FAPI	5	6.1	1.3-16.3	
Medial shaft bone (Includes skull, ribs, and spine)	FDG	5	7.25	1.1-12.5	0.470
	FAPI	8	9.15	1.3-18.8	

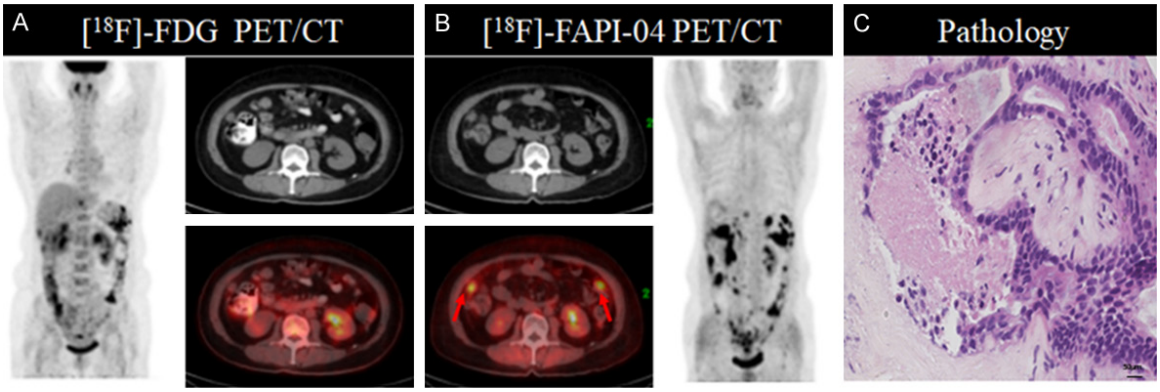

Figure 6. Detection results of abdominal metastatic tumor. A 64-year-old woman was admitted with a 2-month history of abdominal distention. Abdominal ultrasound revealed a predominant abdominal mass, which was suspected to be malignant. Further evaluation with [18F]-FDG PET/CT and [18F]-FAPI-04 PET/CT was performed before treatment. A. FDG: No abnormal radioactive distribution is seen. B. FAPI: Nodular shadow is seen in bilateral paracolic sulcus, SUVmax: 5.9. C. Surgical pathology shows intra-retinal adenocarcinoma, Scale bar, 50 μm.

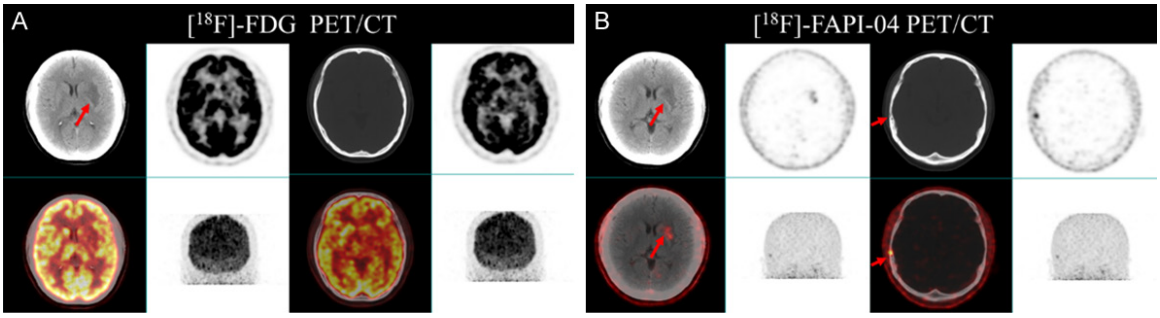

Figure 7. Detection results of head metastatic tumor. A 45-year-old female hospitalized with a 3-month history of cough and malaise. Chest CT revealed a dense shadow in the lower lobe of the right lung. Following anti-inflammatory treatment, a repeat CT scan was performed, and malignancy was suspected. Further evaluation with [18F]-FDG PET/CT and [18F]-FAPI-04 PET/CT was performed before treatment. A. FDG: Slightly hypodense nodule in the deep left frontal lobe, abnormal radioactive concentration in PET, SUVmax: 7.6. No abnormalities in bony structures. B. FAPI: Slightly hypodense nodule with abnormal radiolucency of PET seen in the deep left frontal lobe SUVmax: 2.1. Abnormal concentration in the right temporal bone SUVmax: 6.2.

Table 6. Diagnostic value of [18F]-FAPI-04 PET/CT and [18F]-FDG PET/CT in bone and visceral metastases

Basis of analysis and modality	Sensitivity (%) 95% CI	Specificity (%) 95% CI	PPV (%) 95% CI	NPV (%) 95% CI	Accuracy (%) 95% CI
[18F]-FDG PET/CT	60.71 (17/28)	55.56 (10/18)	68.0 (17/25)	47.62 (10/21)	58.7 (27/46)
	40.7-77.9	31.3-77.6	46.4-84.3	26.4-69.7	43.2-73.0
[18F]-FAPI-04 PET/CT	82.14 (23/28)	44.44 (8/18)	69.7 (23/33)	61.54 (8/13)	67.39 (31/46)
	62.4-93.2	22.4-68.6	51.1-83.8	32.3-84.9	51.9-80.4
P-value	0.076	0.505	0.890	0.429	0.388

Note: The numbers in brackets are the number of lesions used to calculate the percentage CI confidence interval. PPV: positive predictive value, NPV: negative predictive value.

Table 7. Results of the 3-dimensional paired chi-square test for the comparison of lymph node involvement

Item	Sensitivity		Specificity	
	McNemar Test	Kappa	McNemar Test	Kappa
[18F]-FDG PET/CT vs. [18F]-FAPI-04 PET/CT	P=0.031	0.503	P=0.500	0.780

be attributed to the enhanced uptake of [18F]-AIF-NOTA-FAPI-04. Pancreatic, hepatocellular (both cholangiocellular and hepatocellular), sarcoma, esophageal, and gastric cancers showed the highest uptake of [18F]-AIF-NOTA-FAPI-04, reflecting their strong connective tissue proliferative response [12]. Five primary tumors were not revealed by [18F]-FDG PET/CT in our investigation. It is suggested that the application of [18F]-FDG PET/CT is limited in certain tumors, such as hepatocellular carcinoma, gastric cancer, and pancreatic cancer. The tracer that can be used to detect other tumors in [18F]-FDG PET/CT has not been found yet, and it still needs to be explored in the future.

Due to the limitation of [18F]-FDG, [18F]-AIF-NOTA-FAPI-04 may be a new potential method for PET/CT. However, it was also noted that the tumor specificity of [18F]-FDG was higher than that of [18F]-AIF-NOTA-FAPI-04. In the present study, one patient with pancreatic cancer failed to show significant positive uptake in [18F]-AIF-NOTA-FAPI-04 PET/CT scan due to excessive uptake throughout the pancreas caused by neoplastic pancreatitis, which hid the tumor uptake of [18F]-AIF-NOTA-FAPI-04. Therefore, extra attention must be paid when reading [18F]-AIF-NOTA-FAPI-04 images of tumors with combined inflammation. It has been found that tumor size can affect the [18F]-FDG PET visibility of primary tumors. Visibility is poor for extremely tiny lesions (<1.0 cm) because of partial volume impacts and limited tumor metabolic activity [13, 14]. Tiny tumors (<1.0 cm in diameter) that were missed by [18F]-FDG PET/CT were visualized by [18F]-AIF-NOTA-FAPI-04 PET/CT in the present investigation. Thus, [18F]-AIF-NOTA-FAPI-04 PET/CT may complement [18F]-FDG PET/CT to recognize small malignant lesions.

Compared with [18F]-FDG PET/CT, [18F]-AIF-NOTA-FAPI-04 PET/CT showed more positive lymph nodes in the supraclavicular, cervical, mediastinal and abdominal areas. The results of this study showed that the sensitivity of [18F]-FDG PET/CT for the identification of metastatic lymph nodes was low. The high sensitivity of [18F]-AIF-NOTA-FAPI-04 PET/CT in detecting lymph nodes addresses the limitations of PET/CT. This is particularly relevant in cases where lymph node staging using [18F]-FDG PET/CT has shown low to moderate sensitivity, such as in esophageal, gastric, and prostate cancers [15-17]. This study noted that increased tracer uptake may lead to more false-positive lymph node uptake, resulting in lower specificity of [18F]-AIF-NOTA-FAPI-04 PET/CT. However, the difference was not statistically significant. In several cases of false positive by [18F]-FDG PET/CT, we found no abnormal uptake in mediastinal and hilar lymph nodes with [18F]-AIF-NOTA-FPI-04 PET/CT. Therefore, [18F]-AIF-NOTA-FPI-04 PET/CT may be an effective method to assess lymph node status and prevent unnecessary interventions before treatment.

The abnormal foci in the brain, omentum, mesentery, peritoneum, axial skeleton, and liver

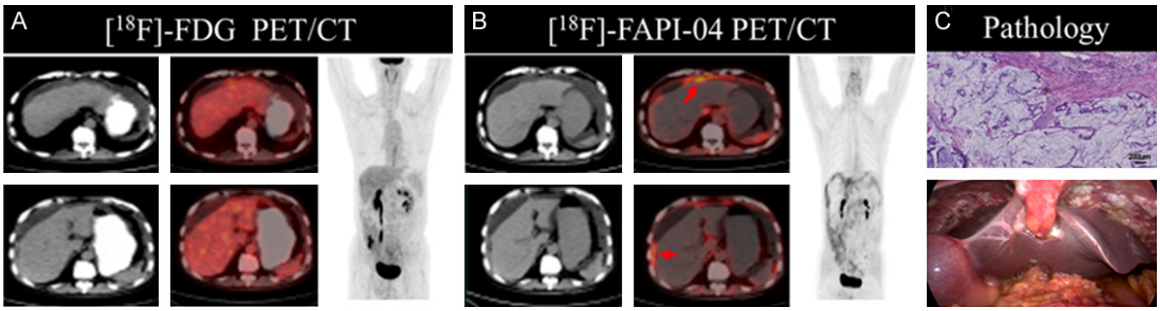

Figure 8. Detection results of a case of omental mucinous adenocarcinoma. A 65-year-old man was admitted with a hernia and elevated CA199 levels. During colonoscopy, access could not be achieved 20 cm from the anus. A CT scan of the whole abdomen was performed, showing a cystic solid occupancy in the appendix area. Further evaluation with [18F]-FDG PET/CT and [18F]-FAPI-04 PET/CT was performed before treatment. A. FDG: Wall peritoneum, no abnormal radioactive distribution. B. FAPI: Wall peritoneal thickening, showing abnormal radioactive concentration, SUVmax: 4.3. C. Surgical pathology shows mucinous adenocarcinoma of the greater omentum, Scale bar, 200 μm.

were less in [18F]-FDG PET/CT scans than those in [18F]-AIF-NOTA-FAPI-04 PET/CT scans when determining visceral and bone metastases. The sensitivity of [18F]-FDG PET/CT was significantly lower in comparison with that of [18F]-AIF-NOTA-FAPI-04 PET/CT in detecting visceral and bone metastases. In contrast, the false-positive results produced by [18F]-FDG PET/CT was less than [18F]-AIF-NOTA-FAPI-04 PET/CT. Most of the false results were from diseases with activated fibrotic response, such as cirrhosis, myelofibrosis, and sarcoidosis. In such cases, CT scans can differentiate benign from malignant tumors.

This study also found that [18F]-AIF-NOTA-FAPI-04 was superior to [18F]-FDG for recognizing liver metastases, peritoneal cancer, and brain tumors in PET/CT. Liver is a target organ for many metastatic cancers, including pancreatic, colorectal, and gastric cancers. It is known that [18F]-FDG PET/CT has low sensitivity for detecting tiny liver metastases (lower than 1 cm), leading to false-negative findings [18]. In the current investigation, liver absorption of [18F]-AIF-NOTA-FAPI-04 was substantially lower than that of [18F]-FDG. This modest background activity may contribute to detecting metastases in the liver. Peritoneal metastatic cancer is a common form of metastasis of ovarian and gastrointestinal tumors, and its detection is a key determinant of treatment [19]. However, [18F]-FDG PET/CT has a low sensitivity for detecting peritoneal cancer and has limited use in staging and surgical planning [20, 21]. In contrast to [18F]-FDG, [18F]-AIF-NOTA-FAPI-04 does not physiologically accumulate in the intestine. Consequently, non-specific uptake in the peritoneal cavity is quite low [22]. More importantly, the uptake of [18F]-FDG was lower than that of [18F]-AIF-NOTA-FAPI-04 in patients with peritoneal cancer, allowing for clear visualization of visceral peritoneal, mesenteric, and omental involvement with extremely elevated contrast (**Figure 8**). This finding provides a basis for further study of using [18F]-AIF-NOTA-FAPI-04 PET/CT to detect the peritoneal dissemination of ovarian and gastrointestinal tumors.

This study is limited in its ability to analyze the diagnostic efficacy of specific tumor types based on a comparative subgroup analysis because of the small number of patients with each type of cancer. Therefore, we analyzed primary and metastatic lesions from multiple cancer types in a pooled manner. Due to this selection bias, our cohort may not be a representative group of cancer patients. Furthermore, the patients underwent two examination methods, [18F]-AIF-NOTA-FAPI-04 PET/CT and [18F]-FDG PET/CT, which may also cause certain bias, even though there were at least one week interval between these two examinations to minimize the possible impact. Moreover, [18F]-AIF-NOTA-FAPI-04 imaging is mainly based on the overexpression of αVβ3 and αVβ5 integrin on the surface of tumor cells, while [18F]-FDG PET detects the difference in metabolic activity between tumor cells and surrounding normal tissues. Although the imaging principles of the two types of PET/CT are different, the deviation of the test results is small. In addition, pathological confirmation of abnormal [18F]-AIF-NOTA-FAPI-04 and [18F]-FDG uptake did not just serve to validate PET/CT results. To confirm the diagnosis, biopsies were carried out on lesions sus-

pected to be malignant (the oncologist selected the biopsy targets based on PET/CT results of [18F]-FDG and [18F]-AIF-NOTA-FAPI-04). Thus, the actual specificity might be lower than we have reported.

Conclusion

According to this study, [18F]-AIF-NOTA-FAPI-04 PET/CT allows for effective visualization of primary tumors, as well as most tumor involvement in various types of cancer patients. In the liver and abdomen tumors, [18F]-AIF-NOTA-FAPI-04 uptake is strong due to the low background uptake. [18F]-AIF-NOTA-FAPI-04 PET/CT offers superior sensitivity and accuracy to [18F]-FDG PET/CT in detecting primary and metastatic lesions. In contrast, in comparison with the [18F]-FDG PET/CT, the [18F]-AIF-NOTA-FAPI-04 produced higher false-positive results, leading to a lower specificity for metastatic lesion detection (no statistically significant difference was noted).

Acknowledgements

This paper is supported by Provincial Key Research and Development Program of Heilongjiang Province (GA21C001) (KW).

Disclosure of conflict of interest

None.

Address correspondence to: Kezheng Wang, Department of PET-CT/MRI, Harbin Medical University, Harbin Medical University Cancer Hospital, No. 150 Haping Road, Nangang District, Harbin 150081, Heilongjiang, China. Tel: +86-0451-85718900; E-mail: wangkezheng9954001@163.com

References

[1] Altmann A, Haberkorn U and Siveke J. The latest developments in imaging of fibroblast activation protein. J Nucl Med 2021; 62: 160-167.

[2] Meyer C, Dahlbom M, Lindner T, Vauclin S, Mona C, Slavik R, Czernin J, Haberkorn U and Calais J. Radiation dosimetry and biodistribution of 68Ga-FAPI-46 PET imaging in cancer patients. J Nucl Med 2020; 61: 1171-1177.

[3] Lindner T, Loktev A, Giesel F, Kratochwil C, Altmann A and Haberkorn U. Targeting of activated fibroblasts for imaging and therapy. EJNMMI Radiopharm Chem 2019; 4: 16.

[4] Loktev A, Lindner T, Mier W, Debus J, Altmann A, Jäger D, Giesel F, Kratochwil C, Barthe P, Roumestand C and Haberkorn U. A tumor-imaging method targeting cancer-associated fibroblasts. J Nucl Med 2018; 59: 1423-1429.

[5] Lamprecht S, Sigal-Batikoff I, Shany S, Abu-Freha N, Ling E, Delinasios GJ, Moyal-Atias K, Delinasios JG and Fich A. Teaming up for trouble: cancer cells, transforming growth factor-β1 signaling and the epigenetic corruption of stromal naïve fibroblasts. Cancers (Basel) 2018; 10: 61.

[6] Bu L, Baba H, Yoshida N, Miyake K, Yasuda T, Uchihara T, Tan P and Ishimoto T. Biological heterogeneity and versatility of cancer-associated fibroblasts in the tumor microenvironment. Oncogene 2019; 38: 4887-4901.

[7] Hamson EJ, Keane FM, Tholen S, Schilling O and Gorrell MD. Understanding fibroblast activation protein (FAP): substrates, activities, expression and targeting for cancer therapy. Proteomics Clin Appl 2014; 8: 454-463.

[8] Siveke JT. Fibroblast-activating protein: targeting the roots of the tumor microenvironment. J Nucl Med 2018; 59: 1412-1414.

[9] Wikberg ML, Edin S, Lundberg IV, Van Guelpen B, Dahlin AM, Rutegård J, Stenling R, Oberg A and Palmqvist R. High intratumoral expression of fibroblast activation protein (FAP) in colon cancer is associated with poorer patient prognosis. Tumour Biol 2013; 34: 1013-1020.

[10] Rettig WJ, Su SL, Fortunato SR, Scanlan MJ, Raj BK, Garin-Chesa P, Healey JH and Old LJ. Fibroblast activation protein: purification, epitope mapping and induction by growth factors. Int J Cancer 1994; 58: 385-392.

[11] Wang S, Zhou X, Xu X, Ding J, Liu S, Hou X, Li N, Zhu H and Yang Z. Clinical translational evaluation of Al18F-NOTA-FAPI for fibroblast activation protein-targeted tumour imaging. Eur J Nucl Med Mol Imaging 2021; 48: 4259-4271.

[12] Kratochwil C, Flechsig P, Lindner T, Abderrahim L, Altmann A, Mier W, Adeberg S, Rathke H, Röhrich M, Winter H, Plinkert PK, Marme F, Lang M, Kauczor HU, Jäger D, Debus J, Haberkorn U and Giesel FL. 68Ga-FAPI PET/CT: tracer uptake in 28 different kinds of cancer. J Nucl Med 2019; 60: 801-805.

[13] Spadafora M, Pace L, Evangelista L, Mansi L, Del Prete F, Saladini G, Miletto P, Fanti S, Del Vecchio S, Guerra L, Pepe G, Peluso G, Nicolai E, Storto G, Ferdeghini M, Giordano A, Farsad M, Schillaci O, Gridelli C and Cuocolo A. Risk-related 18F-FDG PET/CT and new diagnostic strategies in patients with solitary pulmonary nodule: the ITALIAN multicenter trial. Eur J Nucl Med Mol Imaging 2018; 45: 1908-1914.

[14] Redondo-Cerezo E, Martínez-Cara JG, Jiménez-Rosales R, Valverde-López F, Caballero-Mateos A, Jérvez-Puente P, Ariza-Fernández JL, Úbeda-Muñoz M, López-de-Hierro M and de Teresa J.

Endoscopic ultrasound in gastric cancer staging before and after neoadjuvant chemotherapy. A comparison with PET-CT in a clinical series. United European Gastroenterol J 2017; 5: 641-647.

[15] Jiang C, Chen Y, Zhu Y and Xu Y. Systematic review and meta-analysis of the accuracy of ^{18}F-FDG PET/CT for detection of regional lymph node metastasis in esophageal squamous cell carcinoma. J Thorac Dis 2018; 10: 6066-6076.

[16] Jadvar H. Is there use for FDG-PET in prostate cancer? Semin Nucl Med 2016; 46: 502-506.

[17] Findlay JM, Antonowicz S, Segaran A, El Kafsi J, Zhang A, Bradley KM, Gillies RS, Maynard ND and Middleton MR. Routinely staging gastric cancer with ^{18}F-FDG PET-CT detects additional metastases and predicts early recurrence and death after surgery. Eur Radiol 2019; 29: 2490-2498.

[18] Sivesgaard K, Larsen LP, Sørensen M, Kramer S, Schlander S, Amanavicius N, Bharadwaz A, Tønner Nielsen D, Viborg Mortensen F and Morre Pedersen E. Diagnostic accuracy of CE-CT, MRI and FDG PET/CT for detecting colorectal cancer liver metastases in patients considered eligible for hepatic resection and/or local ablation. Eur Radiol 2018; 28: 4735-4747.

[19] Coccolini F, Gheza F, Lotti M, Virzì S, Iusco D, Ghermandi C, Melotti R, Baiocchi G, Giulini SM, Ansaloni L and Catena F. Peritoneal carcinomatosis. World J Gastroenterol 2013; 19: 6979-6994.

[20] Shimada H, Okazumi S, Koyama M and Murakami K. Japanese gastric cancer association task force for research promotion: clinical utility of ^{18}F-fluoro-2-deoxyglucose positron emission tomography in gastric cancer. A systematic review of the literature. Gastric Cancer 2011; 14: 13-21.

[21] Rubini G, Altini C, Notaristefano A, Merenda N, Rubini D, Ianora AA and Asabella AN. Role of ^{18}F-FDG PET/CT in diagnosing peritoneal carcinomatosis in the restaging of patient with ovarian cancer as compared to contrast enhanced CT and tumor marker Ca-125. Rev Esp Med Nucl Imagen Mol 2014; 33: 22-27.

[22] Li M, Younis MH, Zhang Y, Cai W and Lan X. Clinical summary of fibroblast activation protein inhibitor-based radiopharmaceuticals: cancer and beyond. Eur J Nucl Med Mol Imaging 2022; 49: 2844-2868.